PHYSICAL REVIEW A VOLUME 56, NUMBER 2 AUGUST 1997

Spectrum of the ion-trap laser

Georg M. Meyer, Markus Löffler, and Herbert Walther
Max-Planck-Institut für Quantenoptik, Hans-Kopfermann-Strasse 1, D-85748 Garching, Germany
and Sektion Physik, Ludwig-Maximilians-Universität, München, Germany
(Received 2 April 1997)

The spectral properties of the ion-trap laser [Europhys. Lett. **37**, 317 (1997)] are investigated for a realistic multilevel scheme containing a Λ-type subsystem. In the laser region, the linewidth of the output spectrum is up to ten times smaller than the cavity damping rate and roughly proportional to the inverse of the mean photon number. Significant modifications and photon antibunching occur for thresholdless lasing. The fluorescence spectrum displays the signature of the coherently scattered resonator field. [S1050-2947(97)50608-1]

PACS number(s): 42.50.−p, 32.80.−t, 42.55.−f

Recently, an experimental setup has been proposed that allows for laser operation with a single Ca^+ ion in a high-finesse optical resonator [1,2]. With the help of an ion trap, the charged atom can be kept in permanent interaction with the cavity field. The resulting dynamics of this one-atom laser [3–5] is very different from the one in the microlaser [6], where a sequence of prepared atoms traverses the resonator.

It has been pointed out that the ion-trap laser can produce light with Poissonian and even sub-Poissonian statistics. The coherently pumped system shows the formation of two thresholds. In general, as in conventional lasers, a certain pump strength is needed to drive the system above threshold. The second threshold is due to the dynamic Stark effect, which moves the atomic system out of resonance with the cavity mode if the coherent pump is too strong. Between these two thresholds, lasing occurs. For certain pump parameters, the first threshold disappears, and there is thresholdless lasing [7].

In this Rapid Communication, we investigate the spectral properties of such a microscopic laser system. So far, output and fluorescence spectra have only been examined in idealized two-level models [4,8]. After elaborating on the details of the Ca^+ scheme, we study the output and fluorescence spectra of the ion-trap laser. New spectral features and photon antibunching [9], not found in the two-level laser, are observed in the region of thresholdless lasing.

The setup under investigation is the ion-trap laser as proposed in Refs. [1,2]. The active medium consists of one single $^{40}Ca^+$ ion, which is kept in an endcap trap [10]. It is difficult to find a laser transition in the frequency range where high-finesse resonators [11] are available. In addition, the need for a pump scheme with appropriate transition rates and frequencies excludes most ions. The pump scheme for Ca^+ is illustrated in Fig. 1(a). As the laser transition we use $|4\,P_{1/2}\rangle \leftrightarrow |3\,D_{3/2}\rangle$ with the wavelength $\lambda = 866$ nm. A coherent field couples the ground state $|4\,S_{1/2}\rangle$ to the upper laser level $|4\,P_{1/2}\rangle$. This pump transition, which has already been used for laser cooling [12], and the laser transition form a Λ-type subsystem. The coherent pump induces, together with the resonator field, atomic coherences between the levels $|4\,S_{1/2}\rangle$ and $|3\,D_{3/2}\rangle$, which support laser action. Furthermore, two incoherent (broadband) pumps with bidirectional rates Γ_1 and Γ_2 on the transitions $|3\,D_{3/2}\rangle \leftrightarrow |4\,P_{3/2}\rangle$ and $|3\,D_{5/2}\rangle \leftrightarrow |4\,P_{3/2}\rangle$, respectively, are needed to complete the pump cycle and to prevent the population from collecting in metastable states (pockets).

To treat the system in a realistic way, one has to consider the polarizations of the laser and pump fields as well as the Zeeman sublevels of the fine structure. Therefore, *a priori*, we have a multilevel scheme with 18 levels. We assume the resonator mode (g) and the coherent pump field (Ω) to be linearly polarized and the incoherent pump fields (Γ_1 and Γ_2) to be unpolarized. By grouping the sublevels, which can be labeled by their magnetic quantum number m_J, the 18-level scheme can be reduced to an eight-level system, as indicated in Fig. 1(b). The pump fields are distinguished by different types of arrows. Atomic decay is represented by dashed arrows; for clarity, these are not shown on the laser and pump transitions. The decay rates between the groups of sublevels follow from the Clebsch-Gordon coefficients between the Zeeman components and are given in Fig. 1(c). To illustrate the grouping for the laser transition, the corresponding Zeeman substructure is depicted in Fig. 1(d). For example, the relative decay rate from the upper laser level $|4\,P_{1/2}\rangle$ to the lower laser level $|3\,D_{3/2}, \pm 1/2\rangle$ is given by $1/3 + 1/6 = 1/2$. In order to calculate the atom-field coupling one has to use the relative coupling strength 1/3 instead of 1/2, as can be seen in Fig. 1(d).

It has been discussed in Refs. [1,2] that with the help of the pump-operator method [13] the system can be reduced further to an effective three-level system whose dynamics is governed by a non-Markovian master equation. This simplifies the numerical calculation of the statistical properties of the multilevel system.

We are here primarily interested in the dynamical properties and treat the problem numerically for the eight-level system by direct integration of the master equation

$$\frac{\partial}{\partial t}\rho = \frac{1}{i\hbar}[H,\rho] + L_{\text{field}}\rho + L_{\text{atom}}\rho = \mathcal{L}\rho \tag{1}$$

for the density operator ρ of the atom-field system. The Hamilton operator

$$H = -\hbar g(a\sigma^\dagger + a^\dagger\sigma) - \hbar\Omega(|4\,S_{1/2}\rangle\langle 4\,P_{1/2}| + \text{H.c.}) \tag{2}$$

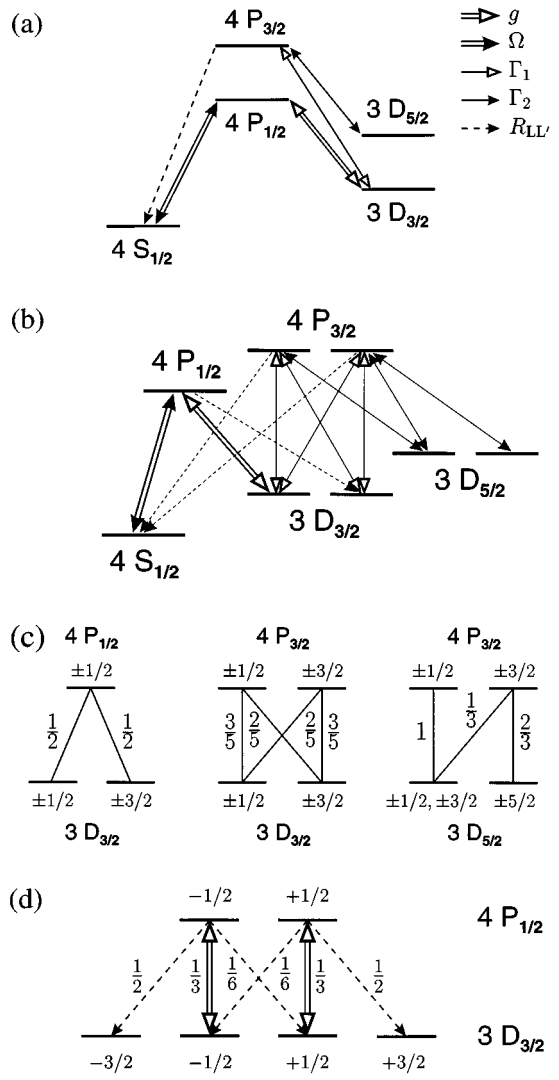

FIG. 1. (a) Schematic representation of the Ca^+ scheme as proposed in Ref. [1]. (b) A more detailed look at the pump and decay channels. The grouping of the magnetic sublevels is given in (c) together with the relative decay rates between the groups. (d) Zeeman sublevels and relative coupling strengths on the laser transition $|4P_{1/2}\rangle \leftrightarrow |3D_{3/2}\rangle$.

describes the coupling of the atom to the quantized laser mode with coupling strength g and to the coherent pump field with Rabi frequency 2Ω. The lowering operator on the laser transition is denoted by $\sigma = |3D_{3/2}, \pm 1/2\rangle\langle 4P_{1/2}|$, the photon annihilation operator by a. The losses of the cavity are described by

$$L_{\text{field}}\rho = -\frac{A}{2}(a^\dagger a\rho + \rho a^\dagger a - 2a\rho a^\dagger) \tag{3}$$

with the damping rate A. Relaxation processes as well as incoherent pumping are given by L_{atom}. In Fig. 1, the rate for a transition from level $|\mathrm{L}\rangle$ to $|\mathrm{L}'\rangle$ is designated $R_{\mathrm{LL}'}$.

We study two kinds of spectra: the spectrum of the photons emitted through the cavity mirrors, here called *output* spectrum $S_a(\omega)$, and the spectrum of the photons emitted out the sides of the cavity, the *fluorescence* spectrum $S_\sigma(\omega)$. They are defined as

$$S_a(\omega) = \int_0^\infty \mathrm{d}\tau \cos[(\omega-\omega_0)\tau] g_a^{(1)}(\tau), \tag{4}$$

$$S_\sigma(\omega) = \int_0^\infty \mathrm{d}\tau \cos[(\omega-\omega_0)\tau] g_\sigma^{(1)}(\tau), \tag{5}$$

where ω is the frequency of the resonator field and ω_0 is the atomic frequency of the laser transition. The normalized first-order correlation functions are given by

$$g_a^{(1)}(\tau) = \lim_{t\to\infty} \frac{\langle a^\dagger(t+\tau)a(t)\rangle}{\langle a^\dagger(t)a(t)\rangle} = \frac{\mathrm{Tr}\{a^\dagger \mathrm{e}^{\mathcal{L}\tau} a\rho^{(\mathrm{ss})}\}}{\mathrm{Tr}\{a^\dagger a\rho^{(\mathrm{ss})}\}}, \tag{6}$$

$$g_\sigma^{(1)}(\tau) = \lim_{t\to\infty} \frac{\langle \sigma^\dagger(t+\tau)\sigma(t)\rangle}{\langle \sigma^\dagger(t)\sigma(t)\rangle} = \frac{\mathrm{Tr}\{\sigma^\dagger \mathrm{e}^{\mathcal{L}\tau} \sigma\rho^{(\mathrm{ss})}\}}{\mathrm{Tr}\{\sigma^\dagger \sigma\rho^{(\mathrm{ss})}\}}, \tag{7}$$

where $\rho^{(\mathrm{ss})}$ is the atom-field density matrix in the steady state and $\mathcal{L}$ is the total Liouville operator.

For the calculation, the same parameters as in Ref. [1] are used, i.e., $A=1$ MHz, $g=14.8$ MHz, $\Gamma_1=40$ MHz, and $\Gamma_2=100$ MHz. These parameters could be realized, for example, in a symmetric optical resonator with the length $L=1$ mm, the beam waist $w_0=25$ μm, and the finesse $\mathcal{F}=10^6$. Similar resonators have been used in Refs. [6,11]. Furthermore, the decay rates $R_{\mathrm{LL}'}$ for Ca^+ (as listed in Ref. [1]) are taken into account.

Figure 2(a) shows a plot of the output spectrum for different Rabi frequencies of the coherent pump field. For convenience, we have introduced $\Delta = \omega - \omega_0$. Lasing is most pronounced for $\Omega \approx 50$ MHz with a photon flux of $\langle a^\dagger a\rangle A \approx 6\times 1$ MHz. The output spectrum is particularly narrow in this parameter region, and its shape is Lorentzian. Below the first threshold and above the second threshold, the spectrum is much broader and deviates from a Lorentzian. The dependency of the full width at half maximum (FWHM) of the output spectrum on the coherent pump strength Ω is shown in Fig. 2(b) together with the mean photon number. The linewidth is found to be approximately proportional to $\langle a^\dagger a\rangle^{-1}$. In the laser region, the linewidth is about 0.1 MHz, which is a factor of 10 smaller than the photon damping rate A.

The corresponding fluorescence spectrum for $\Omega=50$ MHz is plotted in Fig. 3(a). It is dominated by a narrow elastic peak at center frequency on top of an inelastic background. Only part of the peak, which has the same width as the output spectrum, is shown in the plot. The origin of this peak is the following: the photons of the laser mode are elastically scattered off the very same atom they were generated by. Even if the finesse of the resonator is ten times worse, i.e., $A=10$ MHz, the elastic peak is still visible, as shown by the dashed curve in Fig. 3(a). For larger values of Ω, sidebands due to the dynamic Stark splitting are resolved; see Fig. 3(b). The emergence of this Autler-Townes doublet [14] goes hand in hand with the vanishing of laser action.

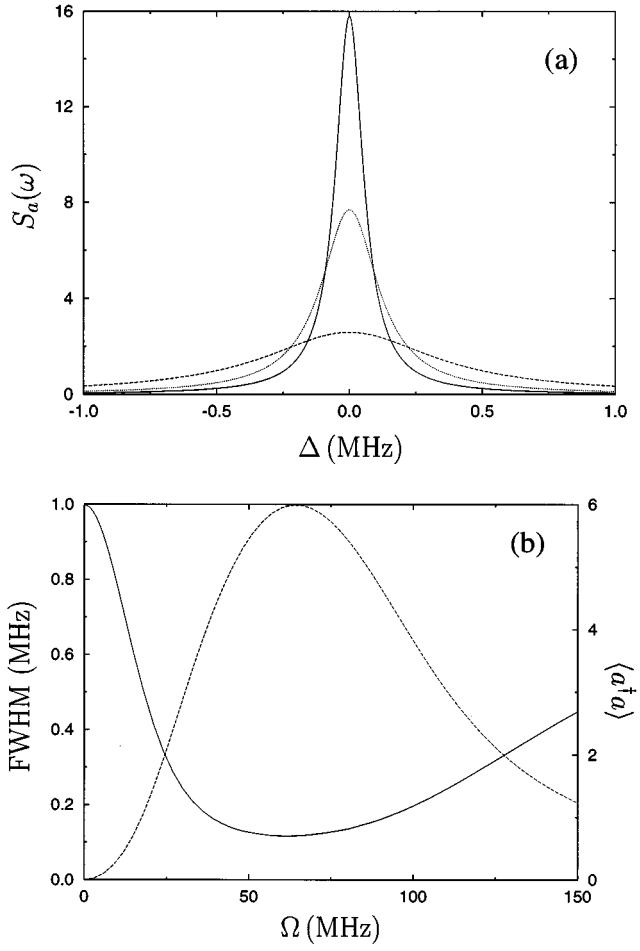

FIG. 2. (a) Output spectrum $S_a(\omega)$ for $\Omega = 10$ MHz (dashed line), $\Omega = 50$ MHz (solid line), and $\Omega = 110$ MHz (dotted line). The other parameters are $g = 14.8$ MHz, $A = 1$ MHz, $\Gamma_1 = 40$ MHz, and $\Gamma_2 = 100$ MHz. (b) Linewidth (FWHM, solid line) and mean photon number ($\langle a^\dagger a \rangle$, dashed line) versus Ω.

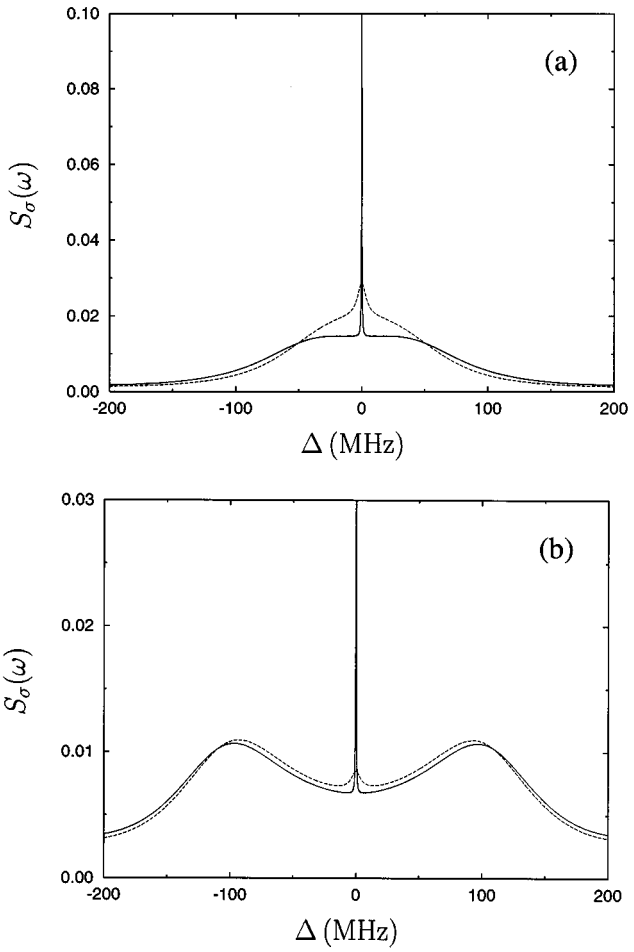

FIG. 3. Fluorescence spectrum $S_\sigma(\omega)$ for the cavity damping rates $A = 1$ MHz (solid line) and $A = 10$ MHz (dashed line). The coherent pump strength is (a) $\Omega = 50$ MHz and (b) $\Omega = 110$ MHz. The other parameters are as in Fig. 2.

For small values of Γ_1, the photon statistics becomes sub-Poissonian and the first threshold disappears [as shown in Fig. 4(b) of Ref. [1]]. Nevertheless, laser light with a photon distribution as in Fig. 4 is produced. The second-order correlation function

$$g_a^{(2)}(\tau) = \lim_{t\to\infty} \frac{\langle a^\dagger(t) a^\dagger(t+\tau) a(t+\tau) a(t)\rangle}{\langle a^\dagger(t) a(t)\rangle^2}, \qquad (8)$$

as depicted in Fig. 4, displays photon antibunching for thresholdless lasing and photon bunching for two-threshold lasing.

Figure 5 shows the linewidth of the output spectrum and the mean photon number in the parameter region of thresholdless lasing, illustrating two new features. First, the output can have very different linewidths for the same intensity, e.g., for $\Omega = 8$ MHz and $\Omega = 138$ MHz we find $\langle a^\dagger a \rangle = 0.2$ (i.e., an output flux of 2×10^5 photons per second), but FWHM $= 0.5$ MHz and FWHM $= 0.8$ MHz, respectively. This behavior is due to the fact that $\Omega = 8$ MHz lies in the linear gain region and $\Omega = 138$ MHz is already beyond the second threshold. In the presence of two thresholds, however, the minimum of the linewidth and the maximum of the

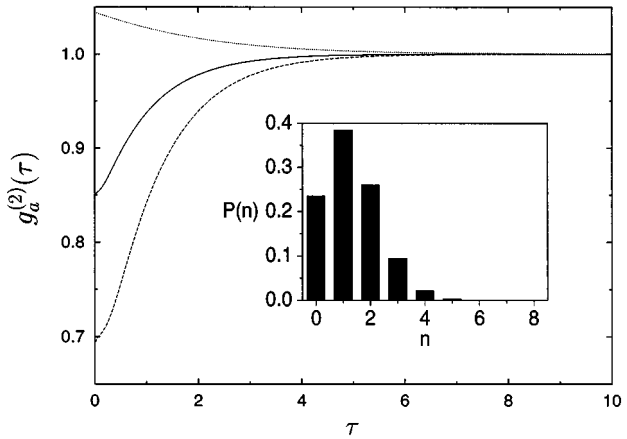

FIG. 4. The correlation function $g_a^{(2)}(\tau)$ shows antibunching for thresholdless lasing with $\Gamma_1 = 5$ MHz, $\Omega = 20$ MHz (solid line), $\Gamma_1 = 1$ MHz, $\Omega = 20$ MHz (dashed line) and bunching for two-threshold lasing with $\Gamma_1 = 40$ MHz, $\Omega = 50$ MHz (dotted line). The other parameters are as in Fig. 2. The photon distribution in the inset corresponds to the solid curve.

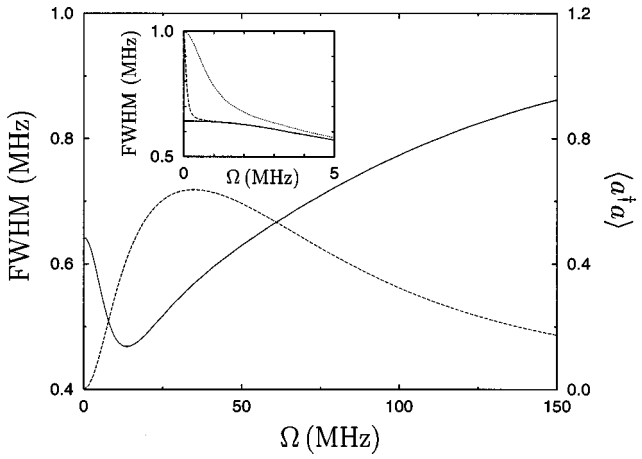

FIG. 5. Linewidth of the output spectrum (solid line) and mean photon number (dashed line) for $\Gamma_1 = 1$ MHz. The other parameters are as in Fig. 2. The inset shows the dependence on the number of thermal photons: $\nu = 0$ (solid line), $\nu = 10^{-4}$ (dashed line), and $\nu = 10^{-2}$ (dotted line).

mean photon number occur for nearly the same Ω, as in Fig. 2(b), and the feature mentioned above is not found.

Second, for $\Omega \to 0$, the linewidth seems to approach a value that is substantially smaller than the cavity decay rate $A = 1$ MHz. This is in contrast to the situation of Fig. 2(b). However, for very small Ω, the linewidth depends critically on the number of thermal photons ν. In the presence of thermal photons, the resonator field approaches the thermal state and the linewidth is given by A for vanishing Ω. The transition from the behavior for $\nu \neq 0$ to $\nu = 0$ for very small Ω can be inferred from the inset of Fig. 5. For small ν, the linewidth shows first a steep decrease from FWHM $= A$ for increasing Ω and then a plateau. The smaller the value of ν, the steeper the decrease. In the limit $\nu \to 0$, the linewidth versus Ω approaches a step function. For the present resonator mode ($\lambda = 866$ nm) at room temperature ($T = 300$ K), the number of thermal photons is $\nu \approx 10^{-24}$. The linewidth in the plateau region depends on the width of the metastable lower laser level, which is broadened by the incoherent pump Γ_1.

To summarize, we have investigated the spectral properties of the ion-trap laser. In the laser region between the two thresholds, a narrow laser line has been found. The signature of the generated resonator field can also be seen in the fluorescence spectrum, even for a cavity which is ten times worse than the one envisioned. In the region of thresholdless lasing, the dynamical properties are found to be qualitatively different from the two-threshold situation. The present calculations are relevant for an experimental realization of the ion-trap laser.

[1] G. M. Meyer, H.-J. Briegel, and H. Walther, Europhys. Lett. **37**, 317 (1997).

[2] G. M. Meyer, doctoral thesis, University of Munich, 1996 (unpublished).

[3] Y. Mu and C. M. Savage, Phys. Rev. A **46**, 5944 (1992).

[4] C. Ginzel, H.-J. Briegel, U. Martini, B.-G. Englert, and A. Schenzle, Phys. Rev. A **48**, 732 (1993).

[5] T. Pellizzari and H. Ritsch, J. Mod. Opt. **41**, 609 (1994).

[6] K. An, J. J. Childs, R. R. Dasari, and M. S. Feld, Phys. Rev. Lett. **73**, 3375 (1994).

[7] Semiconductor microlasers with thresholdless or low-threshold lasing are reviewed in Y. Yamamoto and R. E. Slusher, Phys. Today **46** (6), 66 (1993).

[8] M. Löffler, G. M. Meyer, and H. Walther, Phys. Rev. A **55**, 3923 (1997).

[9] W. Vogel and D.-G. Welsch, *Lectures on Quantum Optics* (Akademie, Berlin, 1997).

[10] C. A. Schrama, E. Peik, W. W. Smith, and H. Walther, Opt. Commun. **101**, 32 (1993).

[11] H. J. Kimble, in *Cavity Quantum Electrodynamics*, edited by P. R. Berman (Academic, Boston, 1994), p. 203.

[12] S. Urabe, M. Watanabe, H. Imajo, and K. Hayasaka, Opt. Lett. **17**, 1140 (1992).

[13] H.-J. Briegel, G. M. Meyer, and B.-G. Englert, Phys. Rev. A **53**, 1143 (1996); Europhys. Lett. **33**, 515 (1996).

[14] S. H. Autler and C. H. Townes, Phys. Rev. **100**, 703 (1955).